

Article

Spatial Variability and Factors Influencing the Air-Sea N₂O Flux in the Bering Sea, Chukchi Sea and Chukchi Abyssal Plain

Man Wu, Liqi Chen *, Liyang Zhan *, Jiexia Zhang, Yuhong Li and Jian Liu

Key Laboratory of Global Change and Marine-Atmospheric Chemistry (GCMAC) of State Oceanic Administration (SOA), Third Institute of Oceanography (TIO), SOA, Xiamen 361005, China; wuman@tio.org.cn (M.W.); zhangjiexia@tio.org.cn (J.Z.); liyuhong@tio.org.cn (Y.L.); liujianhgd@163.com (J.L.)

* Correspondence: Chenliqi@tio.org.cn (L.C.); zhanliyang@tio.org.cn (L.Z.)

Academic Editor: Huiting Mao

Received: 29 December 2016; Accepted: 18 March 2017; Published: 24 March 2017

Abstract: The concentrations of the ozone-depleting greenhouse gas nitrous oxide (N₂O) in the upper 300 m of the Subarctic and Arctic Oceans determined during the 5th Chinese National Arctic Research Expedition were studied. The surface water samples revealed that the study area could be divided into three regions according to the distribution of dissolved N₂O in the surface water, namely, the Aleutian Basin (52° N–60° N), continental shelf (60° N–73° N) and Canadian Basin (north of 73° N), with N₂O in the surface water in equilibrium, oversaturated and undersaturated relative to the atmosphere, respectively. The influences of physical and chemical processes, such as eddy diffusion and sedimentary emissions, beneath the surface layer are discussed. The results of a flux evaluation show that the Aleutian Basin may be a weak N₂O source of approximately $0.46 \pm 0.1 \mu\text{mol}\cdot\text{m}^{-2}\cdot\text{d}^{-1}$, and the continental shelf acts as a strong N₂O source of approximately $8.2 \pm 1.4 \mu\text{mol}\cdot\text{m}^{-2}\cdot\text{d}^{-1}$. By contrast, the Chukchi Abyssal Plain (CAP) of the Canadian Basin is at least a temporal N₂O sink with a strength of approximately $-10.2 \pm 1.4 \mu\text{mol}\cdot\text{m}^{-2}\cdot\text{d}^{-1}$.

Keywords: N₂O; Arctic Oceans; air-sea flux

1. Introduction

Nitrous oxide (N₂O) is an important atmospheric trace gas that is one of the most powerful greenhouse gases in the troposphere with a radiative forcing efficiency 200–300 times greater per molecule than that of CO₂ [1]. In addition, N₂O is a major precursor of ozone-depleting nitric oxide radicals in the stratosphere. The atmospheric concentration of N₂O has been increasing significantly since pre-industrial times [2]. N₂O is considered the most important ozone-depleting substance due to its increased emissions, while the emissions of other major ozone-depleting substances (e.g., chlorofluoro carbon) have decreased over time [3].

The ocean plays a key role in regulating the climate via the exchange of energy and matter with the atmosphere. For N₂O, the ocean acts as one of the most important sources to the atmosphere, contributing $\sim 4 \text{ Tg}\cdot\text{N N}_2\text{O a}^{-1}$, or $\sim 1/3$ of the annual natural N₂O source [4–6]. In situ observations of N₂O concentrations have covered large areas of the world's oceans and determined that surface waters contain $\sim 3\%$ more N₂O than the equilibrium concentration on average [4]. Significant N₂O sources have been found in the tropical ocean where upwelling occurs, for example, in the Peruvian upwelling system of the subtropical Pacific Ocean [7] and in the Arabian Sea [8], which contribute $\sim 0.2\text{--}0.9 \text{ Tg N a}^{-1}$ and $\sim 0.5\text{--}1 \text{ Tg N a}^{-1}$, respectively. Other studies of oceanic N₂O can be found in the review by Bange [9]. However, the contributions of regions such as the Arctic Ocean, where relevant data are scarce, to the atmospheric reservoir are not well known, and only a few studies on this topic

have been conducted to date. Hirota, et al. [10] reported an oversaturation of N₂O in the Bering and Chukchi Seas, and Kitidis et al. [11] noted both surface oversaturation and undersaturation of N₂O along the Arctic Northwest Passage. Zhan, Chen, Zhang and Li [7] suggested that the deep Canadian Basin retains a pre-industrial N₂O signal and further discovered that the Greenland Basin is a sink for N₂O [12]; Zhang et al. [13] revealed the coexistence of oversaturation and undersaturation in the water column of the western Arctic Ocean and a possible mechanism for N₂O production but did not evaluate the magnitudes of sources and sinks. The sea ice coverage over the Arctic Ocean has continued to decrease, and it reached a historic minimum in 2012. Given the retreat of sea ice and exposure of sea water in the Arctic Ocean, the source and sink characteristics of this ocean and its role in the global N₂O budget must be addressed.

In this study, the N₂O data obtained during the 5th Chinese National Arctic Research Expedition (CHINARE) in the upper 300 m of the Bering Sea (including the Aleutian Basin and Bering Sea continental Shelf), Bering Strait, Chukchi Sea and Canadian Basin are presented. The distribution of the surface N₂O concentration and saturation state, as well as the factors of influence, are discussed, and the air-sea N₂O flux is evaluated.

2. Methods and Study Region

2.1. Methods

The method used for the dissolved N₂O measurements was described in detail by Zhan et al. [14]. Briefly, water samples were collected following the methods described by Butler and Elkins [15], and subsamples were collected in 250 mL BOD bottles from 10 L Niskin bottles attached to an SBE 911 conductivity, temperature and depth (CTD) sensor. Each sample was gradually filled from the bottom and allowed to overflow for approximately 2–3 volumes of the bottle. A greased ground-glass stopper was inserted after amendment with 180 µL of saturated HgCl₂ solution, and the bottle was then sealed using a clip. Water samples were stored at 4 °C in the dark until analysis. During analysis, each water sample was transferred into a 20 mL headspace vial, which was then clamped using an iron clamp with a silicone rubber septa. A bubble-free subsample was required before headspace introduction. Approximately 12 mL of the water sample was replaced with ultrahigh purity nitrogen (99.999%). The headspace sample was then transferred to the agitator of a CTC autosampler and equilibrated at 45 °C with 700 rounds per minute for 10 min. After achieving full equilibrium, 1 mL of the headspace sample was injected into a Shimadzu[®] gas chromatography with electron capture detector (GC-ECD) device. References were also prepared according to the procedure described by Zhan, Chen, Zhang and Lin [14]. Since atmospheric N₂O is stable and can be used as a reference according to Butler and Elkins [15], reference water samples were prepared by equilibrating the HgCl₂ solution (1 L) to the ambient atmosphere in a Thermo[®] thermostatic circulation water bath. The water temperature was held at 25 °C (temperature precision of 0.01 °C). No N₂O source was identified in the laboratory, and ambient N₂O mixing only involved atmospheric N₂O. Then, 12 mL of headspace was created by introducing N₂O gas certified references (100, 400, 700, 1500 and 4000 ppb N₂O) to create a gradient. The certificated references were provided by the National Institute of Metrology, P.R. China, and the relative expanded uncertainty of the standards was <5% based on intercalibration with NOAA references. A water-gas mixing reference was used to eliminate possible error, and the details of this approach were reported by Zhan, Chen, Zhang and Lin [14]. With this method, the uncertainty of the data was estimated to be approximately ±2%.

2.2. Study Region and Hydrographic Setting

The data in this study were obtained during CHINARE 5 from July to September 2012. Figure 1 shows the study area, which covers the Aleutian Basin, Bering Sea Continental Shelf, Bering Strait, Chukchi Sea and Chukchi Abyssal Plain (CAP). The Aleutian Basin, Bering Sea Continental Shelf, Bering Strait and Chukchi Sea were investigated during July when the R/V Xuelong headed for the

Arctic Ocean, whereas the CAP was investigated during September when the R/V Xuelong returned to China.

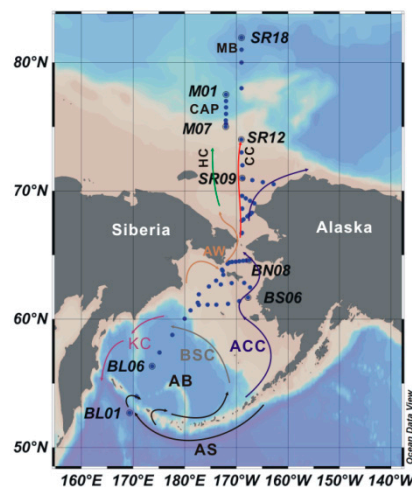


Figure 1. Stations of the 5th Chinese National Arctic Research Expedition (CHINARE) investigated in this study. AB is the Aleutian Basin, CAP is the Chukchi Abyssal Plain, MB is the Makarov Basin, HC is Herald Canyon, and CC is the Central Channel. The currents are marked with different colors: black for the Alaskan Stream (AS), blue for the Alaskan Coastal Current (ACC), purple for the Kamchatka Current (KC), gray for the Bering Slope Current (BSC), and brown for Anadyr Water (AW). Three branches are located north of the Bering Strait: the west branch, middle branch and east branch, which are marked in green, red and blue, respectively, from west to east.

The Aleutian Basin is dominated by a cyclonic gyre that is strongly influenced by the Alaskan Stream, which enters the Aleutian Basin via several passages in the Aleutian Arc, turns east along the Alaskan Arc, forms the Bering Slope Current, and turns south to form the Kamchatka Current. Part of the Bering Slope Current overflows onto the Bering Shelf and enters the Arctic Ocean as a result of the gradient that exists between the Pacific and Arctic Oceans. The inflow water is separated into three branches, which flow, in turn, from west to east through Herald Canyon and the Central Channel between the Herald and Hanna Shoals with the Alaska Coastal Current (ACC) [16]. The west branch is influenced by Anadyr Water (AW) and is characterized by low temperature (T ranges between -1.0 and 1.5 °C), high salinity ($S > 32.5$ psu) and high nutrient concentrations, whereas the east branch water is influenced by the high-temperature ($T > 4$ °C), low-salinity ($S < 31.8$ psu), and nutrient-depleted ACC. The middle branch is characterized by a blending of the physical and chemical characteristics of the east and west branches [17,18]. Judging from the locations of the stations and the hydrographical characteristics (Figure 2), our study area may be affected more by AW than the ACC.

In the western Arctic Ocean, several layers of water are present in the upper 500 m. The surface mixed layer (SML) lies in the upper 20 m and consists of warm (-1.2 to 8.8 °C) and fresh (26.2–31.2) water that results from sea ice melting and riverine discharge. Below the SML, a temperature maximum (< -1.0 °C) occurs as a result of summer Bering Sea Water or Alaskan Coastal Water (ACW) [19]. Arctic Halocline Water is located beneath these layers. Upper Halocline Water (UHW) (70–150 m) consists of Pacific Summer Water (PSW) and Pacific Winter Water (PWW), which are characterized by salinities of $31.0 < S < 33.0$ and 33.0 [20], respectively, whereas Lower Halocline Water (LHW), which originates on the Eurasian shelf [21], is located at approximately 250 m and characterized by a salinity and temperature of 33.8 – 34.4 °C and -0.8 °C, respectively [22].

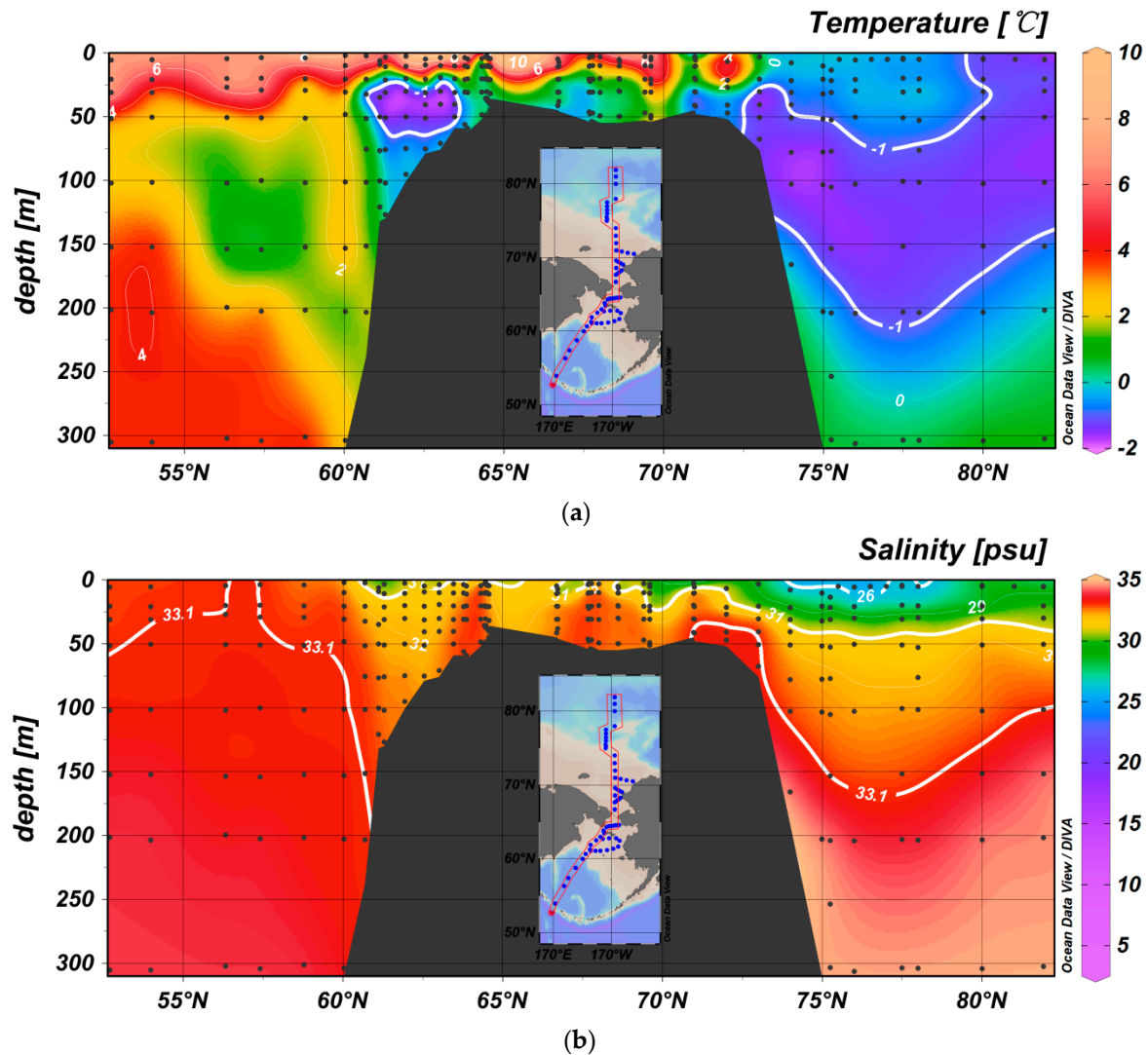


Figure 2. Temperature and salinity distributions in the study area. (a) Flow of Pacific water into the Arctic Ocean via the Bering Strait, resulting in a cold halocline water layer with a minimum temperature of approximately $-1.5\text{ }^{\circ}\text{C}$ located at approximately 100–150 m in the Canadian Basin. A similar cold-water core is also located above the Bering Sea Continental Shelf, likely resulting from winter convection. (b) The upper halocline consists of Pacific Summer Water (PSW) with a salinity of 31–32 and Pacific Winter Water (PWW) with a salinity centered at approximately 33 in the Canadian Basin.

2.3. Saturation Anomaly

To account for the temperature effect on N_2O solubility, the N_2O partial pressure difference, or Saturation Anomaly (SA), is used instead of concentrations to illustrate potential source or sink characteristics in certain regions. SA can be calculated using Equation (1):

$$\text{SA} = \frac{C_{ob} - C_{eq}}{C_{eq}} \times 100 \quad (1)$$

where C_{ob} is the observed N_2O concentration and C_{eq} is calculated using the contemporary atmospheric N_2O mixing ratio at the time of sampling (available at www.esrl.noaa.gov/gmd/hats) according to the method proposed by Weiss and Price [23].

2.4. Calculation of Eddy Diffusion

The following formula can be used to evaluate the contribution of subsurface water to surface water:

$$F_h = K_h \left(\frac{d_{N_2O}}{d_Z} \right) \quad (2)$$

where F_h is the diffusion flux; K_h is the eddy diffusion coefficient; and d_{N_2O} and d_Z are the concentration gradient across the thermocline and the thickness of the thermocline, respectively. In this study, K_h was set to $1.3 \text{ cm}^2/\text{s}$ based on the findings of Li et al. [24].

2.5. Air-Sea Flux Evaluation

The N_2O air-sea flux in the study area was evaluated based on the air-sea model used by Buat-Ménard [25] and other researchers [26,27] and is calculated using Equation (3):

$$F = k\Delta C \quad (3)$$

where the air-sea flux F is the product of k , the piston velocity or exchange coefficient, and ΔC , the gas concentration difference between the atmosphere and surface water.

The different equations for the calculation of k have been summarized by Jiang et al. [28]. Generally, k is proportional to the square or third power of U_{10} (wind speed at 10 m above the sea surface). In this study, the equation proposed by Wanninkhof [27] was used.

$$k = 0.251U_{10}^2 \left(\frac{Sc}{660} \right)^{-\frac{1}{2}} \quad (4)$$

To evaluate the air-sea fluxes in the study area, both in situ wind speed and NCEP reanalysis monthly mean wind speed data (which can be obtained from [29] were used. The monthly mean wind speed data from July were used to evaluate the air-sea flux in the Aleutian Basin and Continental Shelf, and data from September were used for the air-sea flux evaluation of the CAP. Sc can be calculated using the equation proposed by Wanninkhof [27].

$$Sc = 2356.2 - 166.38T + 6.3952T^2 - 0.13422T^3 + 0.0011506T^4 \quad (5)$$

3. Results and Discussion

3.1. Description of N_2O Distribution Patterns in the Surface Water and the Relationship with Regional Source-Sink Characteristics

In this study, the SA was calculated, and it is plotted against latitude in Figure 3. South of 60° N , the lowest N_2O SA in surface water is approximately -2% , which is close to the uncertainty level of our method, suggesting that the surface water in the Aleutian Basin is in equilibrium with the atmosphere since the SA falls within the precision of our method. Oversaturation can be observed over the continental shelf between 60° N and 73° N , with the highest SA of $\sim 30\%$ identified at 65° N . North of 73° N , the surface water of the CAP is undersaturated with respect to N_2O compared to the atmosphere. The lowest SA is $\sim -15\%$. The distribution pattern in this area suggests that the surface water south of 60° N has no obvious N_2O source or sink characteristics, the region between 60° N and 73° N acts as a N_2O source, and the region north of 73° N has characteristics of an N_2O sink. However, to evaluate the air-sea flux, the N_2O distribution pattern of the subsurface layer and its contribution to the surface water must be understood. Therefore, the study area was divided into three areas: the Aleutian Basin, continental shelf (including the Bering Sea Continental Shelf, Bering Strait and Chukchi Sea Shelf), and CAP. Additionally, the distribution of N_2O in subsurface water is discussed in the following sections.

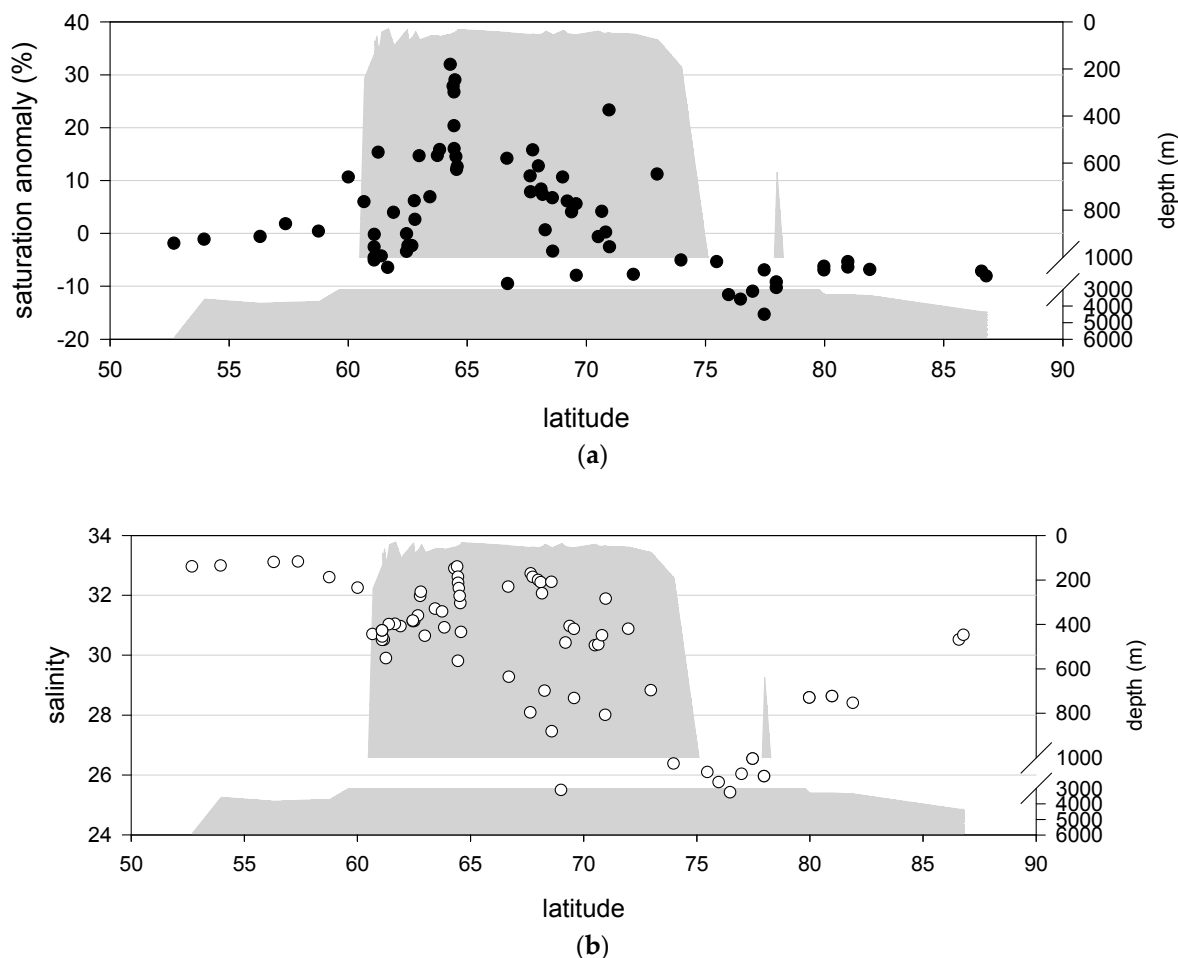


Figure 3. Saturation anomaly and salinity distribution patterns in the surface water of the study area. (a) The SA values show that the N_2O in the surface water between $52^\circ N$ and $60^\circ N$ is in equilibrium with the atmosphere, is oversaturated between $60^\circ N$ and $73^\circ N$ and is undersaturated north of $73^\circ N$. (b) The salinity distribution shows that the minimum salinity identified in the surface water of the study area corresponds to the lowest SA identified in the study area. The bottom depth of the study area is also plotted to indicate the boundaries of subregions.

3.2. Regional Processes that Influence the N_2O Distribution and Air-Sea Fluxes

3.2.1. Aleutian Basin

The Aleutian Basin can be considered part of the Pacific Ocean [30]. The distribution of N_2O in the water column of this basin is similar to that in the Pacific Ocean, with a near-equilibrium N_2O concentration in the surface water and an N_2O maximum at approximately 900 m [31]. Since the surface water is close to equilibrium with the atmosphere, it is generally considered a non-source or non-sink area.

The distribution of N_2O reveals a concentration gradient between the surface water and the depth of the temperature minimum, which suggests that eddy diffusion between these two layers transports the N_2O to the surface layer (Figure 4a,b) and further contributes to the air-sea exchange.

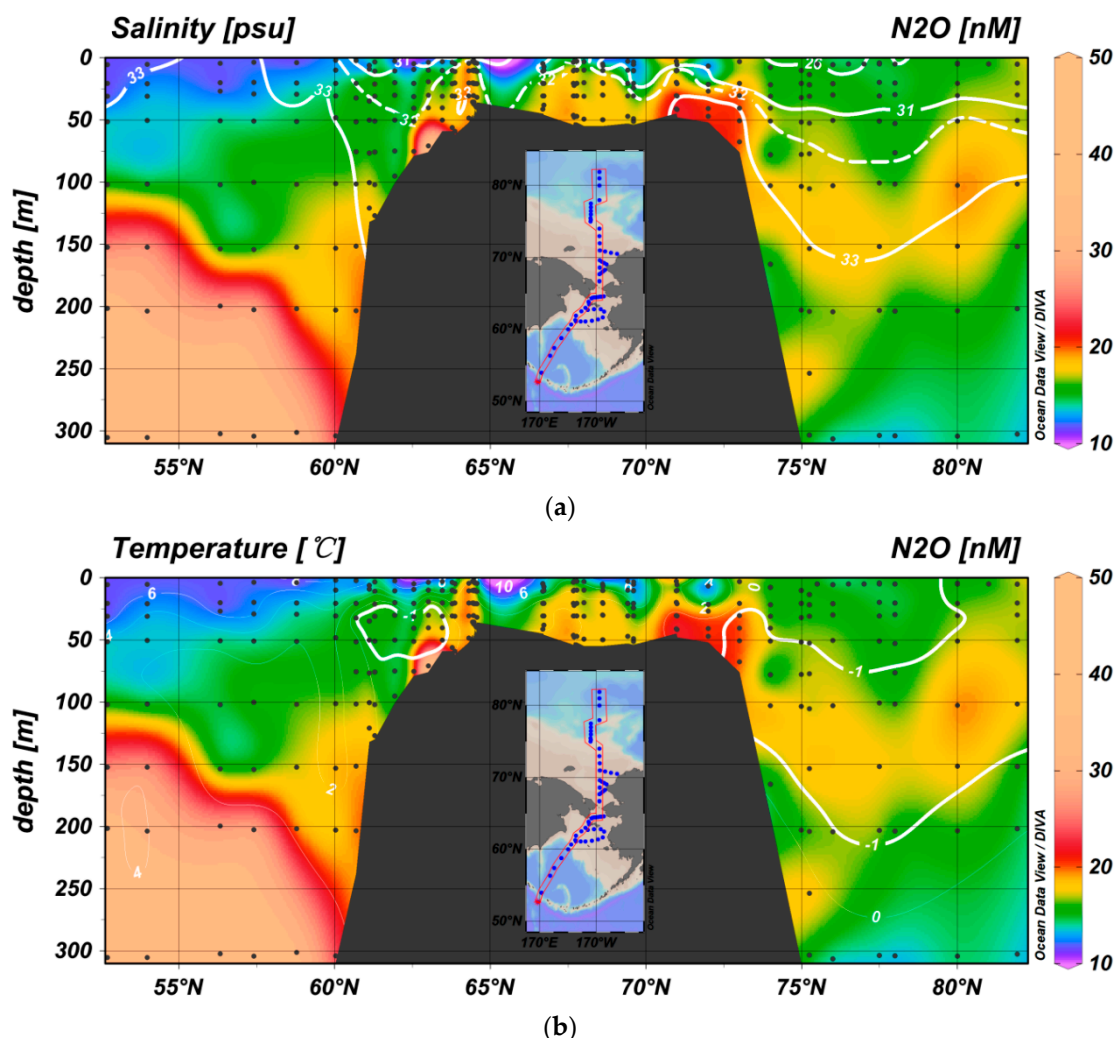


Figure 4. Distribution of N₂O overlying the salinity and temperature distributions. (a) A high N₂O concentration can be identified in the Aleutian Basin and over the Bering Sea Continental Shelf and Chukchi Sea shelf. In the Canadian Basin, a N₂O maximum layer can be identified along the salinity contour of 33. (b) A high N₂O concentration can be identified along the temperature minimum in the Canadian Basin. A similar low temperature center can be observed over the Bering Sea shelf, which is likely a winter remnant and may retain the N₂O signal of Pacific surface water. The N₂O concentration at this temperature minimum, which has not yet been affected by the shelf N₂O maximum, may record the signal of the most recent N₂O concentration in the winter surface water.

In the Aleutian Basin, a temperature minimum is present at a depth of 150 m; therefore, the thermohaline thickness is considered the depth range between the temperature minimum and the bottom of the mixed layer, which is approximately 20 m. In this case, d_z is 130 m, ΔN_2O between these two depths is $\sim 8.1 \text{ nmol}\cdot\text{L}^{-1}$ (with average concentrations of $20.3 \text{ nmol}\cdot\text{L}^{-1}$ and $12.3 \text{ nmol}\cdot\text{L}^{-1}$ at the temperature minimum and mixed layer depth, respectively), and the average F_h of all the stations is $\sim 0.70 \pm 0.06 \text{ }\mu\text{mol}\cdot\text{m}^{-2}\cdot\text{d}^{-1}$. This value is similar to that determined in [31], in which it was suggested that eddy diffusion in the Aleutian Basin is approximately $0.79 \text{ }\mu\text{mol}\cdot\text{m}^{-2}\cdot\text{d}^{-1}$. The air-sea N₂O flux in the Aleutian Basin was then calculated using Equations (4)–(6). In situ wind speed and NCEP reanalysis monthly mean wind speed data were both used to evaluate the air-sea flux, and the results are listed in Table 1. However, we do not assume that the surface water in the Aleutian Basin acts as an N₂O sink because the SA in the surface water is close to the uncertainty of our analytical method. Eddy diffusion contributes approximately $0.70 \pm 0.06 \text{ }\mu\text{mol}\cdot\text{m}^{-2}\cdot\text{d}^{-1}$ to the surface water

and may be a source for the Aleutian Basin. Hence, the near-equilibrium state of the surface water may be due to the rapid exchange of N₂O at the air-sea interface rather than to the transportation of N₂O to the surface water by eddy diffusion, suggesting that the air-sea flux is approximately $0.70 \pm 0.06 \mu\text{mol}\cdot\text{m}^{-2}\cdot\text{d}^{-1}$. However, a strong source result from in situ production may be present in the lower euphotic zone that may also contribute to the atmospheric N₂O reservoir [32]. Toyoda, et al. [33] suggested a source of approximately $1.6 \pm 0.4 \mu\text{mol}\cdot\text{m}^{-2}\cdot\text{d}^{-1}$ in the adjacent western Pacific Ocean. However, such a source was not reflected in the distribution pattern of N₂O. Therefore, one should note that the above estimation may underestimate the N₂O air-sea flux in the Aleutian Basin.

Table 1. Air-sea flux of the study area.

Region	Stations	Longitude	Latitude	Flux 1	Average 1	Flux 2	Average 2
AB	BL01	169.4	52.7	-3.8 ± 0.2	-0.9 ± 1.8	-1.9 ± 0.1	-0.4 ± 1.6
	BL03	170.7	54.0	-0.7 ± 0.5		-1.1 ± 0.7	
	BL06	173.7	56.3	-1.3 ± 6.1		-0.6 ± 3.2	
	BL07	175.1	57.4	1.7 ± 2.1		1.5 ± 1.9	
	BL08	177.6	58.8	0.0 ± 0.1		0.1 ± 1.9	
CS	BL10	180.0	60.0	0.1	9.4 ± 1.2	5.2 ± 1.1	8.2 ± 1.4
	BL12	-178.9	60.7	0.1		3.2 ± 0.9	
	BL13	-177.5	61.3	3.8 ± 0.2		9.1 ± 0.5	
	BL14	-177.3	61.9	0.8 ± 0.6		2.2 ± 1.6	
	BL16	-173.9	63.0	5.4 ± 0.5		9.1 ± 1.0	
	BL15	-175.3	62.5	-0.7 ± 0.8		-1.5 ± 1.7	
	BM01	-172.5	63.5	0.8 ± 0.3		4.6 ± 1.6	
	BM02	-172.6	63.8	13.2 ± 3.2		9.5 ± 2.3	
	BM03	-172.7	63.9	15.5 ± 3.0		10.3 ± 2.0	
	BN01	-171.7	64.3	39.2 ± 0.7		22.2 ± 0.4	
	BN02	-171.4	64.4	53.2 ± 4.4		19.4 ± 1.6	
	BN03	-170.8	64.5	6.2 ± 0.1		13.8 ± 0.3	
	BN04	-170.1	64.5	15.7 ± 2.4		11.1 ± 1.7	
	BN05	-169.4	64.5	51.2 ± 1.9		19.9 ± 0.7	
	BN07	-168.1	64.6	22.3 ± 2.9		8.7 ± 1.1	
	BN08	-167.5	64.6	15 ± 1.9		8.8 ± 1.1	
	R01	-169.0	66.7	5.2 ± 0.6		8.9 ± 1.0	
	R02	-168.9	67.7	1.7 ± 0.5		5.0 ± 1.7	
	CC01	-168.6	67.8	4.3 ± 0.8		10.6 ± 2.1	
	CC03	-167.9	68.0	1.1		8.9 ± 0.4	
CC04	-167.5	68.1	0.5	6.0 ± 0.9			
CC05	-167.3	68.2	0.5 ± 0.3	5.2 ± 3.4			
CC07	-167.0	68.3	0.2 ± 0.1	0.3 ± 0.2			
R03	-168.9	68.6	2.0 ± 0.8	4.7 ± 2.0			
R04	-168.9	69.6	1.7 ± 0.5	4.4 ± 1.5			
C03	-166.5	69.0	0.1	8.4 ± 1.2			
C05	-164.8	70.7	12.5 ± 7.6	3.3 ± 2.0			
C04	-166.9	70.8	0.0 ± 0.7	0.0 ± 1.3			
R05	-168.8	71.0	17.3 ± 1	22.3 ± 1.3			
CAP	SR18	-169.0	81.9	-2.7 ± 0.1	-9.8 ± 1.6	-5.9 ± 0.2	-10.2 ± 1.5
	SR14	-169.0	78.0	-2.7 ± 0.1		-12.7 ± 0.5	
	SR16	-169.0	80.0	-10.3 ± 1.5		-6.7 ± 1.0	
	M01	-172.0	77.5	-3.3 ± 1.1		-8.6 ± 3.0	
	M04	-172.0	76.0	-32.8 ± 3		-13.8 ± 1.2	
	SR12	-169.0	74.0	-1.1 ± 0.2		-6.5 ± 1.3	
	M03	-172.0	76.5	-33.6 ± 3.7		-14.9 ± 1.6	
	M02	-172.0	77.0	-5.7 ± 0.6		-13.5 ± 1.4	
	M05	-172.0	75.5	-11.1 ± 5.0		-6.3 ± 2.8	
	SR17	-169.0	81.0	-1.7 ± 0.2		-6.1 ± 0.7	
	SR16	-169.0	80.0	-11.4 ± 3.3		-7.4 ± 2.1	
M01	-172.0	77.5	-7.4 ± 0.5	-18.8 ± 1.4			

AB is Aleutian Basin; CS is Continental Shelf; and CAP is the Chukchi Abyssal Plain. Flux 1 was calculated using in situ data. Flux 2 was calculated using NCEP reanalysis monthly mean wind speed data. The unit of the air-sea flux is $\mu\text{mol}\cdot\text{m}^{-2}\cdot\text{d}^{-1}$.

3.2.2. Continental Shelf

The continental shelf includes the Bering Slope, Bering Strait and Chukchi Sea and is obviously a strong source of N_2O . As illustrated in Figure 4a,b, high N_2O concentrations were detected along the continental shelf. Two specific locations of high concentrations can be identified at $\sim 63^\circ N$ and $\sim 73^\circ N$, which correspond to two dissolved oxygen minima over the continental shelf (Figure 5). The low dissolved oxygen concentrations over the continental shelf suggest the presence of an oxygen consumption process in the continental shelf sediment. These phenomena over the Bering Sea Continental Shelf and Chukchi Sea continental shelf were observed by Tanaka et al. [34] and Timmermans et al. [35], respectively. These authors considered the oxygen minima over the continental shelf as a result of respiration and nutrient regeneration. Zhang, Zhang, Ren, Li and Liu [13] suggested that denitrification or nitrification in the sediments of these regions may serve as mechanisms of N_2O production over the Chukchi Sea shelf. The N_2O distribution reported based on CHINARE 4 is similar to that from CHINARE 5. Notably, an N^* minimum and high concentrations of NH_4^+ were observed at the oxygen minimum over the continental shelf during CHINARE 4; a similar phenomenon was observed during CHINARE 5 (data unpublished) and can increase nitrification in the water column. High concentrations of NH_4^+ on the Chukchi Sea shelf and its consumption by nitrification were also suggested by Nishino et al. [36]. Therefore, possible denitrification or nitrification in the continental shelf sediments and water column nitrification are likely the mechanisms of N_2O production in the water column.

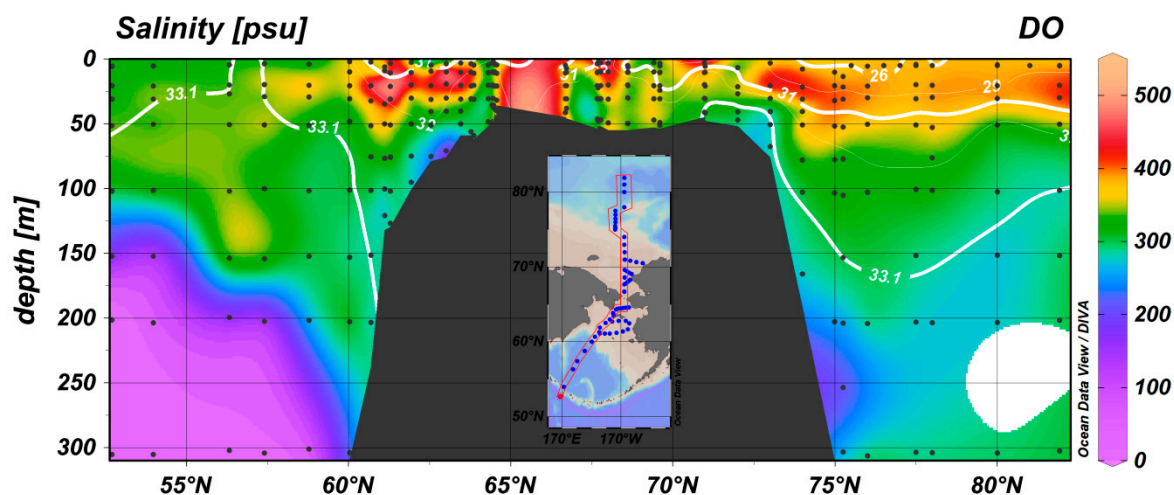


Figure 5. Distribution of dissolved oxygen in the study area. The N_2O concentrations correspond to low-oxygen regions, including the Aleutian Basin, continental shelf and PWW layer.

In addition to these two maxima, the water over the continental shelf has the highest N_2O concentration at the same depth in the entire study region, suggesting that the N_2O production over the continental shelf is the highest in the study area.

The air-sea flux over the continental shelf calculated using Equations (4)–(6) is approximately $8.2 \pm 1.4 \mu\text{mol}\cdot\text{m}^{-2}\cdot\text{d}^{-1}$. This air-sea flux range agrees well with that reported by Hirota, Ijiri, Komatsu, Ohkubo, Nakagawa and Tsunogai [10]. Only 2 of 31 stations over the Bering Sea Continental Shelf exhibited undersaturation and air-to-sea N_2O fluxes, which have SA values close to the method precision of this study; therefore, the Continental Shelf represents a net N_2O source to the atmosphere. Compared to N_2O hotspots such as the Peruvian upwelling system and West Indian Coast, where the sea-to-air N_2O fluxes are approximately $13.1\text{--}30.8 \mu\text{mol}\cdot\text{m}^{-2}\cdot\text{d}^{-1}$ and $40\text{--}268 \mu\text{mol}\cdot\text{m}^{-2}\cdot\text{d}^{-1}$, respectively, the continental shelf air-to-sea flux is not large. However, if the high N_2O concentration over the continental shelf is a general phenomenon over the Arctic Continental shelf, it may provide a significant source in the N_2O budget. Therefore, further investigation is required.

3.2.3. Chukchi Abyssal Plain

The CAP was studied in early September when the sea ice was retreating and the surface water was exposed to the atmosphere. The surface seawater of the CAP was undersaturated with respect to N_2O , with the lowest SA in the entire area. Corresponding to this minimum SA, the lowest salinity was observed at the same latitude, suggesting that the sea ice meltwater affects the surface water salinity, and the minimum SA may be related to sea ice melting. The sea ice formation process likely includes an N_2O outgassing mechanism that is similar to brine rejection. Therefore, the process results in N_2O -depleted meltwater that dilutes the N_2O concentration of the surface water when sea ice melts. Low N_2O concentrations in sea ice have been reported by Randall et al. [37], who found that the N_2O concentration in Arctic sea ice is only $\sim 6 \text{ nmol}\cdot\text{kg}^{-1}$. Additionally, our lab simulation showed that the meltwater from ice made of artificial seawater contains only $\sim 2 \text{ nmol}\cdot\text{L}^{-1}$ (data unpublished). Nishino, Shimada, Itoh, Yamamoto-Kawai and Chiba [20] showed that the melting of sea ice affects the CAP. Therefore, the lowest N_2O SA identified in the CAP area may be related to sea ice melting.

It is assumed that the surface water of the CAP inflows from south of the Bering Strait, with salinity and N_2O levels of 30 and $12.0 \text{ nmol}\cdot\text{L}^{-1}$, respectively. Additionally, the salinity and N_2O levels in the sea ice meltwater are 5 and approximately $6.0 \text{ nmol}\cdot\text{L}^{-1}$, respectively. However, these two end members cannot result in a mixture with a salinity of 26.0 and an N_2O concentration of $15.0 \text{ nmol}\cdot\text{L}^{-1}$ because the sea ice meltwater will lower the salinity and N_2O levels simultaneously. Therefore, the high N_2O concentration in the CAP may result from replenishment by the atmosphere, the waters below or both. In either case, the surface of the CAP plays a role as an N_2O sink from the atmosphere.

An obvious N_2O maximum is present below the CAP surface water. As discussed above, several layers of water exist in the Arctic Ocean, and the hydrographic structure of the CAP is complicated [20]. However, the fine hydrographic structure and its effect on the subsurface N_2O distribution are beyond the scope of this study. Thus, only water masses such as PSW and PWW are considered.

As shown in Figure 2a,b, PSW can be identified by a salinity range of 31–32, and PWW can be identified by salinity centered at 33, both according to Nishino, Shimada, Itoh, Yamamoto-Kawai and Chiba [20]; PWW can also be identified by a temperature minimum. PSW and PWW are Pacific waters that have been modified over the Bering Sea Continental Shelf and Chukchi Sea continental shelf [22,38], as shown in Figure 2a,b. Along the 31–33 salinity contours, the N_2O concentrations in PSW and PWW continue to increase. PSW is believed to originate from the ACW. At station BS06, which is mainly influenced by the ACC, the N_2O concentration in the water is approximately $10.6 \text{ nmol}\cdot\text{L}^{-1}$. This concentration increases to approximately $12.9\text{--}14.6 \text{ nmol}\cdot\text{L}^{-1}$ at station BN08 and then to $\sim 15.1\text{--}16.8 \text{ nmol}\cdot\text{L}^{-1}$ in PSW over the CAP. By contrast, PWW is produced during the winter. Although winter data were unavailable, a cold water mass which is likely the remnant of winter processes can be observed at 62°N and can be considered a PWW end member over the Bering Sea Continental Shelf. The N_2O in this water mass is undersaturated compared to that in the atmosphere, with an average SA of approximately -7.5% , suggesting that this water mass undergoes winter convection before reaching equilibrium with the atmosphere. The N_2O concentration in this cold water mass is approximately $15.3 \text{ nmol}\cdot\text{L}^{-1}$, whereas the N_2O concentration in PWW is approximately 18.1 (range, $17.7\text{--}19.4 \text{ nmol}\cdot\text{L}^{-1}$). Therefore, the N_2O concentration increases in both PSW and PWW may be the result of the modification of the water masses by continental shelf processes. Moreover, because PWW is the main carrier of nutrients from the Chukchi Sea continental shelf, it may also carry N_2O from the continental shelf to the CAP subsurface layer. Local production of N_2O is also possible since the nutrients transported by PWW into the CAP subsurface layer include relatively high concentrations of ammonium [20], which can be oxidized in the water column to form N_2O and contribute to the N_2O budget.

As noted above, the N_2O concentration differs between the thermohaline and the surface water, and N_2O may be transported to the upper layer during summer. Therefore, the eddy diffusion flux should be evaluated. The average eddy diffusion flux of all the stations in the CAP between the

temperature minimum and mixed layer depth (100 m and 20 m) calculated using Equation (2) is approximately $0.27 \pm 0.04 \mu\text{mol}\cdot\text{m}^{-2}\cdot\text{d}^{-1}$.

The air-to-sea N_2O flux in the CAP calculated in this study using Equations (4)–(6) ranges between $-6.0 \pm 0.24 \mu\text{mol}\cdot\text{m}^{-2}\cdot\text{d}^{-1}$ and $-18.9 \pm 1.5 \mu\text{mol}\cdot\text{m}^{-2}\cdot\text{d}^{-1}$, with an average of $-10.2 \pm 1.4 \mu\text{mol}\cdot\text{m}^{-2}\cdot\text{d}^{-1}$, suggesting the presence of an N_2O sink in the central Arctic Ocean. Therefore, compared to the influence of the air-sea flux, the effect of eddy diffusion is negligible.

To date, studies reporting a surface N_2O sink are limited [12,39]. However, we believe that the N_2O sink noted herein is likely temporally variable because of the ice cover during winter, and an oversaturated N_2O water mass is likely present below the N_2O -undersaturated surface water. If the water under the sea ice that has accumulated N_2O is exposed to the atmosphere as the sea ice melts, the area can serve as a temporally variable source in the global N_2O budget.

4. Conclusions

The N_2O fluxes in the Aleutian Basin, continental shelf (including Bering Sea Continental Shelf and, Chukchi Sea) and CAP were studied during CHINARE 5. The Aleutian Basin has source characteristics, with a source strength of approximately $0.46 \pm 0.1 \mu\text{mol}\cdot\text{m}^{-2}\cdot\text{d}^{-1}$. Although the surface water has no obvious source or sink characteristics according to the accuracy of our method, the gradient that exists on both sides of the thermocline suggests that eddy diffusion may be the origin of the local source. The Continental shelf represents a strong regional N_2O source, with an average sea-to-air flux of approximately $8.2 \pm 1.4 \mu\text{mol}\cdot\text{m}^{-2}\cdot\text{d}^{-1}$. This strong source may result from high productivity over the continental shelf, intense respiration and nutrient regeneration in the sediment, and further nitrification in the water column, which suggests that the continental shelf around the Arctic Ocean may act as a significant N_2O source to the atmosphere. In the CAP of the Canadian Basin, although an N_2O maximum is present in subsurface waters, its contribution via eddy diffusion to the surface water is negligible compared to the source strength of the surface water, e.g., approximately $0.25 \pm 0.2 \mu\text{mol}\cdot\text{m}^{-2}\cdot\text{d}^{-1}$ and $-10.4 \pm 1.4 \mu\text{mol}\cdot\text{m}^{-2}\cdot\text{d}^{-1}$. However, the N_2O sink may be a temporal phenomenon, and further analysis is required to address the role that the Arctic Ocean plays in the global N_2O budget.

Acknowledgments: This work was supported by the National Natural Science Foundation of China (grants 41230529, 41676186, and 41506225), the Chinese Projects for Investigations and Assessments of the Arctic and Antarctic (grants CHINARE2012-2017 for 01-4-02, 02-1, 03-04-02, 2016-03-04, and 2016-04-03), and the Chinese International Cooperation Projects (IC201114, IC201201, IC201308, and 2016YFE0103300).

Author Contributions: Liqi Chen and Liyang Zhan conceived and designed the experiments; Yuhong Li and Jian Liu performed the experiments; Jiexia Zhang analyzed the data; Man Wu wrote the paper.

Conflicts of Interest: The authors declare no conflict of interest.

References

1. Khalil, M.A.K.; Rasmussen, R.A.; Shearer, M.J. Atmospheric nitrous oxide: Patterns of global change during recent decades and centuries. *Chemosphere* **2002**, *47*, 807–821. [[CrossRef](#)]
2. Pachauri, R.K.; Allen, M.R.; Barros, V.R.; Broome, J.; Cramer, W.; Christ, R.; Church, J.A.; Clarke, L.; Dahe, Q.; Dasgupta, P. *Climate Change 2014: Synthesis Report. Contribution of Working Groups I, II and III to the Fifth Assessment Report of the Intergovernmental Panel on Climate Change*; Intergovernmental Panel on Climate Change (IPCC): Geneva, Switzerland, 2014.
3. Ravishankara, A.R.; Daniel, J.S.; Portmann, R.W. Nitrous oxide (N_2O): The dominant ozone-depleting substance emitted in the 21st century. *Science* **2009**, *326*, 123–125. [[CrossRef](#)] [[PubMed](#)]
4. Nevison, C.D.; Weiss, R.F.; Erickson, D.J., III. Global oceanic emissions of nitrous oxide. *J. Geophys. Res.* **1995**, *100*, 15809–15820. [[CrossRef](#)]
5. Suntharalingam, P.; Sarmiento, J.L. Factors governing the oceanic nitrous oxide distribution: Simulations with an ocean general circulation model. *Glob. Biogeochem. Cycles* **2000**, *14*, 429–454. [[CrossRef](#)]

6. Freing, A.; Wallace, D.W.R.; Bange, H.W. Global oceanic production of nitrous oxide. *Philos. Trans. R. Soc. Lond. B Biol. Sci.* **2012**, *367*, 1245–1255. [[CrossRef](#)] [[PubMed](#)]
7. Zhan, L.; Chen, L.; Zhang, J.; Li, Y. A vertical gradient of nitrous oxide below the subsurface of the Canada basin and its formation mechanisms. *J. Geophys. Res. Oceans* **2015**, *120*, 2401–2411.
8. Bange, H.W.; Rapsomanikis, S.; Andreae, M.O. Nitrous oxide emissions from the Arabian Sea. *Geophys. Res. Lett.* **1996**, *23*, 3175–3178. [[CrossRef](#)]
9. Bange, H.W. Gaseous nitrogen compounds (NO, N₂O, N₂, NH₃) in the ocean. In *Nitrogen in the Marine Environment*, 2nd ed.; Capone, D.G., Ed.; Elsevier: Amsterdam, The Netherlands, 2008; pp. 55–71.
10. Hirota, A.; Ijiri, A.; Komatsu, D.D.; Ohkubo, S.B.; Nakagawa, F.; Tsunogai, U. Enrichment of nitrous oxide in the water columns in the area of the Bering and Chukchi Seas. *Mar. Chem.* **2009**, *116*, 47–53. [[CrossRef](#)]
11. Kitidis, V.; Upstill-Goddard, R.C.; Anderson, L.G. Methane and nitrous oxide in surface water along the North-West Passage, Arctic Ocean. *Mar. Chem.* **2010**, *121*, 80–86.
12. Zhan, L.; Chen, L.; Zhang, J.; Jinpei, Y.; Li, Y.; Wu, M. A permanent N₂O sink in the Nordic Seas and its strength and possible variability over the past four decades. *J. Geophys. Res. Oceans* **2016**, *121*, 5608–5621. [[CrossRef](#)]
13. Zhang, G.; Zhang, J.; Ren, J.; Li, J.; Liu, S. Distributions and sea-to-air fluxes of methane and nitrous oxide in the North East China Sea in summer. *Mar. Chem.* **2008**, *110*, 42–55. [[CrossRef](#)]
14. Zhan, L.Y.; Chen, L.Q.; Zhang, J.X.; Lin, Q. A system for the automated static headspace analysis of dissolved N₂O in seawater. *Int. J. Environ. Anal. Chem.* **2012**, *93*, 828–842. [[CrossRef](#)]
15. Butler, J.H.; Elkins, J.W. An automated technique for the measurement of dissolved N₂O in natural waters. *Mar. Chem.* **1991**, *34*, 47–61.
16. Woodgate, R.A.; Aagaard, K.; Weingartner, T.J. A year in the physical oceanography of the Chukchi Sea: Moored measurements from autumn 1990–1991. *Deep Sea Res. Part 2* **2005**, *52*, 3116–3149. [[CrossRef](#)]
17. Walsh, J.J.; McRoy, C.P.; Coachman, L.K.; Goering, J.J.; Nihoul, J.J.; Whitedge, T.E.; Blackburn, T.H.; Parker, P.L.; Wirick, C.D.; Shuert, P.G. Carbon and nitrogen cycling within the Bering/Chukchi Seas: Source regions for organic matter effecting AOU demands of the Arctic Ocean. *Prog. Oceanogr.* **1989**, *22*, 277–359. [[CrossRef](#)]
18. Coachman, L.K.; Aagaard, K. Transports through Bering Strait: Annual and interannual variability. *J. Geophys. Res.* **1988**, *93*, 15535–15539. [[CrossRef](#)]
19. Steele, M.; Morison, J.; Ermold, W.; Rigor, I.; Ortmeier, M.; Shimada, K. Circulation of summer Pacific halocline water in the Arctic Ocean. *J. Geophys. Res. Oceans* **2004**. [[CrossRef](#)]
20. Nishino, S.; Shimada, K.; Itoh, M.; Yamamoto-Kawai, M.; Chiba, S. East-west differences in water mass, nutrient, and chlorophyll a distributions in the sea ice reduction region of the western Arctic Ocean. *J. Geophys. Res.* **2008**. [[CrossRef](#)]
21. Jones, E.P.; Anderson, L.G. On the origin of the chemical properties of the Arctic Ocean halocline. *J. Geophys. Res.* **1986**, *91*, 10759–10767. [[CrossRef](#)]
22. Shimada, K.; Itoh, M.; Nishino, S.; McLaughlin, F.; Carmack, E.; Proshutinsky, A. Halocline structure in the Canada basin of the Arctic Ocean. *Geophys. Res. Lett.* **2005**. [[CrossRef](#)]
23. Weiss, R.F.; Price, B.A. Nitrous oxide solubility in water and seawater. *Mar. Chem.* **1980**, *8*, 347–359.
24. Li, Y.H.; Peng, T.H.; Broecker, W.S.; Oestlund, H. The average vertical mixing coefficient for the oceanic thermocline. *Tellus B* **1984**, *36*, 212–217. [[CrossRef](#)]
25. Buat-Ménard, P. Air-sea gas exchange rates: Introduction and synthesis. In *The Role of Air-Sea Exchange in Geochemical Cycling*; Liss, P.S., Ed.; Springer: Dordrecht, The Netherlands, 1986; pp. 113–127.
26. Ho, D.T.; Law, C.S.; Smith, M.J.; Schlosser, P.; Harvey, M.; Hill, P. Measurements of air-sea gas exchange at high wind speeds in the Southern Ocean: Implications for global parameterizations. *Geophys. Res. Lett.* **2006**. [[CrossRef](#)]
27. Wanninkhof, R. Relationship between wind speed and gas exchange. *J. Geophys. Res.* **1992**, *97*, 7373–7382. [[CrossRef](#)]
28. Jiang, L.Q.; Cai, W.J.; Wanninkhof, R.; Wang, Y.; Luger, H. Air-sea CO₂ fluxes on the US South Atlantic Bight: Spatial and seasonal variability. *J. Geophys. Res.* **2008**, *113*, C07019:1–C07019:17. [[CrossRef](#)]
29. Asia-Pacific data-research center. Available online: <http://apdrc.soest.hawaii.edu/data/data.php> (accessed on 9 December 2016).

30. Stabeno, P.J.; Schumacher, J.D.; Ohtani, K. The physical oceanography of the Bering Sea. In *Dynamics of the Bering Sea*; Loughlin, T.R., Ohtani, K., Eds.; University of Alaska Sea Grant: Fairbanks, AK, USA, 1999; pp. 1–28.
31. Chen, L.; Zhang, J.; Zhan, L.; Li, Y.; Sun, H. Differences in nitrous oxide distribution patterns between the Bering Sea basin and Indian Sector of the Southern Ocean. *Acta Oceanol. Sin.* **2014**, *33*, 9–19. [[CrossRef](#)]
32. Dore, J.E.; Popp, B.N.; Karl, D.M.; Sansone, F.J. A large source of atmospheric nitrous oxide from subtropical North Pacific surface waters. *Nature* **1998**, *396*, 63–66.
33. Toyoda, S.; Yoshida, N.; Miwa, T.; Matsui, Y.; Yamagishi, H.; Tsunogai, U.; Nojiri, Y.; Tsurushima, N. Production mechanism and global budget of N₂O inferred from its isotopomers in the western North Pacific. *Geophys. Res. Lett.* **2002**. [[CrossRef](#)]
34. Tanaka, T.; Guo, L.; Deal, C.; Tanaka, N.; Whitley, T.; Murata, A. N deficiency in a well-oxygenated cold bottom water over the Bering Sea shelf: Influence of sedimentary denitrification. *Cont. Shelf Res.* **2004**, *24*, 1271–1283. [[CrossRef](#)]
35. Timmermans, M.L.; Proshutinsky, A.; Golubeva, E.; Jackson, J.M.; Krishfield, R.; McCall, M.; Platov, G.; Toole, J.; Williams, W.; Kikuchi, T.; et al. Mechanisms of Pacific summer water variability in the Arctic's Central Canada basin. *J. Geophys. Res. Oceans* **2014**, *119*, 7523–7548. [[CrossRef](#)]
36. Nishino, S.; Shimada, K.; Itoh, M. Use of ammonium and other nitrogen tracers to investigate the spreading of shelf waters in the western Arctic halocline. *J. Geophys. Res.* **2005**. [[CrossRef](#)]
37. Randall, K.; Scarratt, M.; Levasseur, M.; Michaud, S.; Xie, H.; Gosselin, M. First measurements of nitrous oxide in Arctic Sea ice. *J. Geophys. Res. Oceans* **2012**. [[CrossRef](#)]
38. Woodgate, R.A.; Weingartner, T.J.; Lindsay, R. Observed increases in Bering Strait oceanic fluxes from the Pacific to the Arctic from 2001 to 2011 and their impacts on the Arctic Ocean water column. *Geophys. Res. Lett.* **2012**. [[CrossRef](#)]
39. Hurlburt, H.E.; Wallcraft, A.J. Dynamics of the Kuroshio/Oyashio current system using eddy-resolving models of the North Pacific Ocean. *J. Geophys. Res. Atmos.* **1996**, *101*, 941–976. [[CrossRef](#)]



© 2017 by the authors. Licensee MDPI, Basel, Switzerland. This article is an open access article distributed under the terms and conditions of the Creative Commons Attribution (CC BY) license (<http://creativecommons.org/licenses/by/4.0/>).